

Tight-binding calculations of optical matrix elements for conductivity using nonorthogonal atomic orbitals: Anomalous Hall conductivity in bcc Fe

Chi-Cheng Lee, Yung-Ting Lee, Masahiro Fukuda, and Taisuke Ozaki

Institute for Solid State Physics, The University of Tokyo, 5-1-5 Kashiwanoha, Kashiwa, Chiba 277-8581, Japan

(Received 28 May 2018; revised manuscript received 6 August 2018; published 11 September 2018)

We present a general formula for the tight-binding representation of momentum matrix elements needed for calculating the conductivity based on the Kubo-Greenwood formula using atomic orbitals, which are in general not orthogonal to other orbitals at different sites. In particular, the position matrix element is demonstrated to be important for delivering the exact momentum matrix element. This general formula, applicable to both orthonormal and nonorthonormal bases, solely needs the information of the position matrix elements and the ingredients that have already contained in the tight-binding representation. We then study the anomalous Hall conductivity in the standard example, ferromagnetic bcc Fe, by a first-principles tight-binding Hamiltonian. By assuming the commutation relation $\hat{p} = (im_e/\hbar)[\hat{H}, \hat{r}]$, the obtained frequency-dependent Hall conductivity is found to be in good agreement with existing theoretical and experimental results. Better agreement with experiments can be reached by introducing a reasonable bandwidth renormalization, evidencing the strong correlation among $3d$ orbitals in bcc Fe. Since a tight-binding Hamiltonian can be straightforwardly obtained after finishing a first-principles calculation using atomic basis functions that are generated before the self-consistent calculation, the derived formula is particularly useful for those first-principles calculations.

DOI: [10.1103/PhysRevB.98.115115](https://doi.org/10.1103/PhysRevB.98.115115)

I. INTRODUCTION

In solid-state physics, the introduction of the derivative of the Hamiltonian has many advantages. One famous example is the Hellmann-Feynman theorem, where the derivative of the energy eigenvalue with respect to a parameter λ can be calculated via the expectation value of the derivative of the Hamiltonian with respect to λ . In the first-principles calculations based on density functional theory [1,2], Hellmann-Feynman theorem has been applied for obtaining the forces on nuclei to study ground-state structures and molecular dynamics [3,4]. Another example is the form of the momentum operator for a periodic system, which can be written as the derivative of the Hamiltonian $\hat{H}_u(\vec{k})$ with respect to the crystal momentum \vec{k} . Here, $\hat{H}_u(\vec{k})$ is the Hamiltonian whose eigenfunctions correspond to the cell-periodic parts of Bloch wave functions. This useful expression has been widely adopted to study conductivity, especially in the intrinsic contribution to the anomalous Hall effect that has an intimate relationship to the topology of the electronic structures of studied systems [5–9].

To study the optical conductivity described by a tight-binding Hamiltonian \hat{H} , it is possible to obtain the momentum matrix element by just calculating the derivative of the Hamiltonian matrix element with respect to the crystal momentum \vec{k} in some specific cases [10,11]. Since the properties of basis functions for a tight-binding Hamiltonian obtained from a fitting procedure or a theoretical model are generally unknown and the derivative has a simple form, for example, $te^{i\vec{k}\cdot\vec{R}}$ to $i\vec{R}te^{i\vec{k}\cdot\vec{R}}$, having that all the needed ingredients are already self-contained in the tight-binding representation is attractive and allows for much easier calculations.

However, to study the conductivity with a general set of \hat{H} and bases, one additional term, the position matrix element, needs to be taken into account [12]. For the case having zero onsite contribution due to orbital symmetry together with the fact that the overlaps between intersite orbitals are negligible in the studied system, the position operator sandwiched by atomic orbitals could be neglected, but this approximation needs to be adopted with caution since the intersite position matrix elements are usually non-negligible. The nature of the intra-atomic matrix elements of the position operator can also be understood from the nonorthogonality of the atomic orbitals and could play an important role in some cases [13]. Nevertheless, a general formula for the momentum matrix element expressed by the derivative of Hamiltonian matrix element with respect to \vec{k} and the position matrix element in the bases of atomic orbitals, which are in general not orthogonal to other orbitals at different sites, has not been derived.

The frequency-dependent Hall conductivity in bcc Fe has been studied by first-principles calculations within the generalized gradient approximation (GGA) [14], where good agreement with experiments is found [15,16]. On the other hand, first-principles studies have also shown that bandwidth renormalization needs to be taken into account to compare with the measured quasiparticle bands of bcc Fe in angle-resolved photoelectron spectroscopy experiments [17,18]. It is then interesting to see whether the effect of bandwidth renormalization could give better agreement for the optical conductivity.

In this study, we focus on the tight-binding representation of the momentum matrix elements needed for calculating the optical conductivity based on the Kubo-Greenwood formula

[19–23], which has been of great interest for not only being able to unveil the excited properties of solids but also the connection to the Berry curvature that can reveal the topology of the electronic structures [5–9]. In Sec. II, we will derive the general formula for the momentum matrix elements in the bases of atomic orbitals without assuming the orthonormal relation among all the orbitals. In Sec. III, the results of frequency-dependent Hall conductivity for a standard example, bcc Fe [15,16], will be discussed. Finally, a summary is given in Sec. IV.

II. OPTICAL CONDUCTIVITY

In this section, we will discuss the optical conductivity using the Kubo-Greenwood formula [22] and derive the tight-binding representation of the momentum matrix element, $\langle \vec{k}m | \hat{p} | \vec{k}n \rangle$, in a nonorthonormal basis. While the intraband contribution to the conductivity can solely rely on the knowledge of the tight-binding Hamiltonian ($\langle 0M | \hat{H} | \vec{R}N \rangle$) and the overlap matrix ($\langle 0M | \vec{R}N \rangle$), the interband contribution, similar to the case using an orthonormal basis [7,12], requires the knowledge of the position matrix element, $\langle 0M | \hat{r} | \vec{R}N \rangle$, to deliver the exact conductivity.

A. Kubo-Greenwood formula

The frequency-dependent optical conductivity, $\sigma(\omega)$, expressed by the Kubo-Greenwood formula in the bases of Bloch states can be formulated as

$$\sigma_{\alpha\beta}(\omega) = \frac{-i\hbar}{N_k \Omega} \sum_{\vec{k}mn} \left(\frac{f_{\vec{k}m} - f_{\vec{k}n}}{\epsilon_{\vec{k}m} - \epsilon_{\vec{k}n}} \right) \frac{\langle \vec{k}m | \hat{j}_\alpha | \vec{k}n \rangle \langle \vec{k}n | \hat{j}_\beta | \vec{k}m \rangle}{\omega + \epsilon_{\vec{k}m} - \epsilon_{\vec{k}n} + i\eta}. \quad (1)$$

The current operator \hat{j}_α can be written as the momentum operator $-\hat{p}_\alpha$ in the atomic unit. $f_{\vec{k}n}$ denotes the occupation number of the Bloch state $|\vec{k}n\rangle$ labeled by the crystal momentum \vec{k} and the band index n (lowercase letters) with the energy $\epsilon_{\vec{k}n}$, where the Fermi-Dirac distribution can be applied for $f_{\vec{k}n}$ to introduce the effect of temperature T . The summation of \vec{k} is over the k points inside the first Brillouin zone and the total number of k points is denoted as N_k . The parameter η means 0^+ but is a tunable parameter in practice. Ω denotes the volume of the unit cell. In the case of $\epsilon_{\vec{k}m} \rightarrow \epsilon_{\vec{k}n}$ for the degenerate states or the intraband contribution, $(f_{\vec{k}m} - f_{\vec{k}n})/(\epsilon_{\vec{k}m} - \epsilon_{\vec{k}n})$ should be considered as the derivative of the occupation number with respect to the energy [22], which can be reformulated as $\partial f(\epsilon_{\vec{k}n})/\partial \epsilon_{\vec{k}n}$ with

$$f(\epsilon_{\vec{k}n}) = \frac{1}{e^{(\epsilon_{\vec{k}n} - \mu)/k_B T} + 1}, \quad (2)$$

where μ and k_B are the chemical potential and Boltzmann constant, respectively.

B. Optical matrix element

To study the optical conductivity using Eq. (1), the momentum matrix element, $\langle \vec{k}m | \hat{p} | \vec{k}n \rangle$, needs to be calculated in a basis. Unlike orthonormal basis functions, the atomic orbital $|\vec{R}N\rangle$ labeled by the lattice vector \vec{R} and the orbital index N (capital letters) is in general not orthogonal to the one at

a different site. So the orthonormal relation for the overlap matrix element $S_{\vec{R}'M, \vec{R}N} \equiv \langle \vec{R}'M | \vec{R}N \rangle = \delta_{\vec{R}'R} \delta_{MN}$ does not hold in general. Consequently, the conductivity described by the tight-binding Hamiltonian represented by such basis functions is expected to require the knowledge of $S_{\vec{R}'M, \vec{R}N}$. $S_{\vec{R}'M, \vec{R}N}$ is also expected to be important for calculating the momentum matrix elements.

The energy eigenvalue $\epsilon_{\vec{k}n}$ and the energy eigenstate $|\vec{k}n\rangle$, which is expanded by $\sum_N C_N^{\vec{k}n} |\vec{k}N\rangle$, can be obtained by solving the generalized eigenvalue problem:

$$\sum_N H_{MN}(\vec{k}) C_N^{\vec{k}n} = \epsilon_{\vec{k}n} \sum_N S_{MN}(\vec{k}) C_N^{\vec{k}n}, \quad (3)$$

where $H_{MN}(\vec{k}) \equiv \langle \vec{k}M | \hat{H} | \vec{k}N \rangle$ and $S_{MN}(\vec{k}) \equiv \langle \vec{k}M | \vec{k}N \rangle$. The $\langle \vec{k}n | \hat{p} | \vec{k}n \rangle$ can be derived by first noting that

$$\epsilon_{\vec{k}n} = \sum_{MN} C_M^{\vec{k}n*} H_{MN}(\vec{k}) C_N^{\vec{k}n}. \quad (4)$$

The expectation value of momentum can be obtained by taking the derivative of the energy with respect to \vec{k} . By utilizing Eq. (3) and

$$\frac{\partial}{\partial \vec{k}} \sum_{MN} C_M^{\vec{k}n*} C_N^{\vec{k}n} S_{MN}(\vec{k}) = 0, \quad (5)$$

the derivative of Eq. (4) with respect to \vec{k} can be formulated as

$$\frac{\partial \epsilon_{\vec{k}n}}{\partial \vec{k}} = \sum_{MN} C_M^{\vec{k}n*} C_N^{\vec{k}n} \left(\frac{\partial H_{MN}(\vec{k})}{\partial \vec{k}} - \epsilon_{\vec{k}n} \frac{\partial S_{MN}(\vec{k})}{\partial \vec{k}} \right), \quad (6)$$

where all the needed information besides the solution of Eq. (3) is the Hamiltonian matrix element, $\langle 0M | \hat{H} | \vec{R}N \rangle$, and the overlap matrix element, $\langle 0M | \vec{R}N \rangle$. The resulting formula is expected by considering Hellmann-Feynman theorem for the solution of the generalized eigenvalue problem [24]. Therefore, the intraband contribution, as for the Drude conductivity, can be obtained solely by the knowledge of the tight-binding representation.

We now consider the matrix element for the interband contribution. By assuming the commutation relation $\hat{p} = (im_e/\hbar)[\hat{H}, \hat{r}]$ ($m_e = 1$ and $\hbar = 1$ in the atomic unit) holds for the Hamiltonian \hat{H} , as derived in Appendix A, the momentum operator sandwiched by different energy eigenstates can be formulated as

$$\begin{aligned} \langle \vec{k}m | \hat{p} | \vec{k}n \rangle &= \sum_{MN} C_M^{\vec{k}m*} C_N^{\vec{k}n} \left(\frac{\partial H_{MN}(\vec{k})}{\partial \vec{k}} - \epsilon_{\vec{k}m} \frac{\partial S_{MN}(\vec{k})}{\partial \vec{k}} \right) \\ &+ i(\epsilon_{\vec{k}m} - \epsilon_{\vec{k}n}) \sum_{MN} C_M^{\vec{k}m*} C_N^{\vec{k}n} \sum_{\vec{R}} \langle 0M | \hat{r} | \vec{R}N \rangle e^{i\vec{k} \cdot \vec{R}}, \end{aligned} \quad (7)$$

where additional information, $\langle 0M | \hat{r} | \vec{R}N \rangle$, is needed to deliver the exact value. Although $\langle 0M | \hat{r} | \vec{R}N \rangle$ is origin dependent, the second term of the right-hand side of Eq. (7) is origin independent as discussed in Appendix A. Importantly, the overlap $\langle 0M | \vec{R}N \rangle$ diminishes rapidly before \vec{r} goes to infinity. The importance of such position matrix elements has already been realized for calculating the momentum matrix elements

in an orthonormal basis [7,12]. We also note that the diagonal momentum matrix element, Eq. (6), can be reached by Eq. (7).

C. Discussions

First, we note that Eq. (7), as shown in Appendix A, can be alternatively expressed as

$$\begin{aligned} \langle \vec{k}m | \hat{p} | \vec{k}n \rangle &= i \sum_{MN} C_M^{\vec{k}m*} C_N^{\vec{k}n} \sum_{\vec{R}} \langle 0M | \hat{H} | \vec{R}N \rangle \vec{R} e^{i\vec{k} \cdot \vec{R}} \\ &+ i \epsilon_{\vec{k}m} \sum_{MN} C_M^{\vec{k}m*} C_N^{\vec{k}n} \left(\sum_{\vec{R}} \langle 0N | \hat{r} | \vec{R}M \rangle e^{i\vec{k} \cdot \vec{R}} \right)^* \\ &- i \epsilon_{\vec{k}n} \sum_{MN} C_M^{\vec{k}m*} C_N^{\vec{k}n} \sum_{\vec{R}} \langle 0M | \hat{r} | \vec{R}N \rangle e^{i\vec{k} \cdot \vec{R}}, \end{aligned} \quad (8)$$

where besides the solution of the generalized eigenvalue problem, only the Hamiltonian matrix elements and position matrix elements are required for delivering the exact momentum matrix elements. The overlap matrix element, which was expected to play an important role in a nonorthonormal basis, is not needed explicitly.

Since Eq. (8) is also applicable to an orthonormal basis, the information of position matrix elements is needed to deliver the exact momentum matrix elements even in an orthonormal basis, which can also be found in Eq. (7):

$$\begin{aligned} \langle \vec{k}m | \hat{p} | \vec{k}n \rangle &= \sum_{MN} C_M^{\vec{k}m*} C_N^{\vec{k}n} \frac{\partial H_{MN}(\vec{k})}{\partial \vec{k}} \\ &+ i(\epsilon_{\vec{k}m} - \epsilon_{\vec{k}n}) \sum_{MN} C_M^{\vec{k}m*} C_N^{\vec{k}n} \sum_{\vec{R}} \langle 0M | \hat{r} | \vec{R}N \rangle e^{i\vec{k} \cdot \vec{R}} \end{aligned} \quad (9)$$

for an orthonormal basis. To study $\sigma_{\alpha\beta}$ in the static limit for analyzing the quantized Hall conductance, the momentum matrix element is commonly discussed via the cell-periodic wave function $|u_{\vec{k}n}\rangle$. Recall that the energy eigenstate $|kn\rangle$ can be written in the Bloch form:

$$\Psi_{\vec{k}n}(\vec{r}) = e^{i\vec{k} \cdot \vec{r}} u_{\vec{k}n}(\vec{r}), \quad (10)$$

where the cell-periodic wave function $|u_{\vec{k}n}\rangle$ satisfies

$$\hat{H}_u(\vec{k}) |u_{\vec{k}n}\rangle = \epsilon_{\vec{k}n} |u_{\vec{k}n}\rangle. \quad (11)$$

Thanks to $|u_{\vec{k}n}\rangle$, the momentum matrix element is

$$\langle \vec{k}m | \hat{p} | \vec{k}n \rangle = \langle u_{\vec{k}m} | \frac{\partial \hat{H}_u(\vec{k})}{\partial \vec{k}} | u_{\vec{k}n} \rangle. \quad (12)$$

The famous TKNN (Thouless, Kohmoto, Nightingale, and Nijjs) formula [6] for studying $\sigma_{\alpha\beta}(\omega \rightarrow 0)$ can be derived by utilizing Eq. (12) and then be used to connect to the Berry curvature [5–9]. Since the momentum matrix elements should agree with each other calculated from both methods associated with two different Hamiltonians, the k -dependent position matrix element via Fourier transform as a correction term to $\partial H_{MN}(\vec{k})/\partial \vec{k}$ is essential for delivering the same result of TKNN formula using the Kubo-Greenwood formula by

summing all of the eigenstates of \hat{H} . It is worth mentioning that TKNN formula requires solely the knowledge of occupied bands, which can also be well described by first-principles calculations using atomic basis functions.

Another issue is the commutation relation $\hat{p} = i[\hat{H}, \hat{r}]$, which is assumed to be valid in deriving Eq. (7). For the case where such a relation does not hold, the momentum should be obtained by $\hat{p} = i[\hat{H} - \hat{H}', \hat{r}]$, where the commutator $[\hat{H}', \hat{r}]$ must be taken into account as a correction term to $[\hat{H}, \hat{r}]$ for delivering the exact value of the momentum matrix element. An example of \hat{H}' is the spin-orbit coupling term discussed elsewhere [10] although the correction is estimated to be small. In first-principles calculations, full potentials are commonly replaced by pseudopotentials, and the nonlocal form, $\sum_{lm} |lm\rangle V_{lm} \langle lm|$, which does not commute with \hat{r} in general, is also commonly adopted. The error due to the use of pseudopotentials in calculating momentum matrix elements could be large and depends on the studied systems [25,26]. To reach the solution of a full-potential calculation, for example, $-i \langle \vec{k}n^{\text{full}} | \partial/\partial \vec{r} | \vec{k}n^{\text{full}} \rangle$, from the pseudopotential solution, $-i \langle \vec{k}n^{\text{pseudo}} | \partial/\partial \vec{r} | \vec{k}n^{\text{pseudo}} \rangle$, the addition of projector augmented wave can recover the difference in the wave functions [23]. It can be found that the correction to either the commutation relation or the wave functions could require knowledge way beyond a simple tight-binding representation. Therefore, we propose that Eq. (7) can serve as a good starting point to study the optical conductivity. As we will show in Sec. III, the calculated frequency-dependent conductivity in bcc Fe using Eq. (7) is in good agreement with the reported theoretical results [15,16].

Finally, it should be noted that a limited finite number of atomic basis functions is insufficient to describe a first-principles Hamiltonian. While the Hamiltonian represented by the atomic orbitals could usually give a good description of occupied bands, it is difficult to reproduce accurate unoccupied bands up to a high energy. Therefore, incomplete atomic orbitals could lead to inaccurate frequency-dependent conductivity. For the study of conductivity in bcc Fe, 13 atomic orbitals locating at each atomic site are found to be enough to describe the frequency range we will study in Sec. III. The position operator sandwiched by the energy eigenstates expressed by the atomic orbitals is also expected to deviate from the accurate position matrix element due to the incomplete basis set even without adopting pseudopotentials. However, Eq. (7) is still useful for describing the momentum matrix elements as long as the Hamiltonian represented by the finite number of atomic orbitals can well describe the studied physical quantities. For example, the diagonal momentum matrix element shown in Eq. (7) can deliver accurate Fermi velocity, which is associated with $\partial \epsilon_{\vec{k}n}/\partial \vec{k}$ at the Fermi energy as confirmed by the relationship between Eq. (7) and Eq. (6). Equation (7) and Eq. (6) are obtained from $\hat{p} = i[\hat{H}, \hat{r}]$ and the generalized eigenvalue problem [Eq. (3)], respectively. Obviously, the same $\partial \epsilon_{\vec{k}n}/\partial \vec{k}$ can be reached by the calculations using different kinds of approaches and is measurable by angle-resolved photoelectron spectroscopy experiments. In contrast, a direct calculation of $-i \langle \vec{k}n | \partial/\partial \vec{r} | \vec{k}n \rangle$ could deviate from $\partial \epsilon_{\vec{k}n}/\partial \vec{k}$ noticeably depending on the adopted bases and pseudopotentials.

III. ANOMALOUS HALL CONDUCTIVITY IN BCC FE

For a benchmark calculation, we focus on the anomalous Hall conductivity for the standard example, bcc Fe. The intrinsic contribution to the anomalous Hall conductivity in ferromagnetic bcc Fe has been studied by first-principles calculations using Kubo-Greenwood formula [15], where the results are in good agreement with other theoretical calculations and experiments [27–30]. In this section, we will show the resulting frequency-dependent Hall conductivity using Eq. (7) and compare with the reported conductivity [15,16]. How to reach better agreement between theory and experiment will also be discussed.

A. Computational details

The first-principles calculations were performed using the OpenMX code, [31] where the GGA, the norm-conserving relativistic nonlocal pseudopotentials, and optimized pseudoatomic basis functions were adopted [14,32–34]. The spin-orbit coupling was incorporated through j -dependent pseudopotentials [32]. Two, two, and one optimized radial functions were allocated for the s , p , and d orbitals, respectively, for the Fe atom with a cutoff radius of 6 Bohr. A cutoff energy of 340 Ha was used for numerical integrations and for the solution of the Poisson equation. The $30 \times 30 \times 30$ k -point sampling was adopted for the experimental lattice constant, 2.87 Å. After the self-consistent calculation was done, a tight-binding Hamiltonian in the bases of the 13 adopted pseudoatomic orbitals per Fe atom was obtained and used in calculating the frequency-dependent conductivity using Eqs. (1) and (7), where $\eta = 0.05$ eV and a $150 \times 150 \times 150$ k mesh were chosen. The electronic temperature was set to 300 K for both of the first-principles and conductivity calculations. The magnetization direction is along the z direction.

B. Results

The band structure of ferromagnetic bcc Fe near the Fermi energy including spin-orbit coupling is shown in Fig. 1, where the e_g , t_{2g} , and $s + p$ orbital contributions are presented by blue, red, and green circles, respectively. Two sets of e_g or t_{2g} bands with similar dispersion separated by a large gap (>2 eV at Γ) can be clearly observed and recognized as the spin-up and spin-down bands before being coupled by the spin-orbit coupling. The band structure is consistent with the reported one [15], and therefore the same conductivity is expected to be obtained within density functional theory. Since our formula is based on the Kubo-Greenwood formula involving a summation over all the 13 nonorthogonal pseudoatomic orbitals per Fe atom, a less efficient computation compared with the method using Wannier functions is expected [16]. But it should be noted that the pseudoatomic orbitals are generated before the computation of electronic structure of bcc Fe in comparison with Wannier functions, which need to be constructed after finishing first-principles calculations. All the needed ingredients for Eq. (7) are straightforwardly obtained in our first-principles calculations using the pseudoatomic basis functions, and our tight-binding Hamiltonian shares the same advantage of efficiently calculating the eigenstates at a dense grid of k points needed for describing the Fermi surface

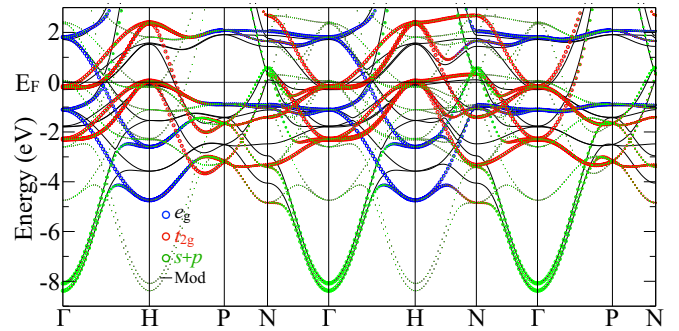


FIG. 1. First-principles band structure of ferromagnetic bcc Fe obtained by adopting 13 pseudoatomic orbitals per Fe atom with spin-orbit coupling. Only the bands near the Fermi energy, which is shifted to zero as denoted by E_F , are shown. Blue and red circles indicate the contribution of Fe $3d$ e_g and t_{2g} orbitals, respectively. The other contribution ($s + p$) is presented by green circles. The modified band structure (Mod) with rescaled hopping integrals between d orbitals (80%) and adjusted onsite energies is presented by the black curves.

of bcc Fe in comparison with the first-principles plane-wave calculations.

The calculated frequency-dependent Hall conductivity using Eqs. (1) and (7) is presented by the black curves in Fig. 2. First, we compare the spectrum of magnetic circular dichroism, which corresponds to the imaginary part of $\omega\sigma_{xy}$,

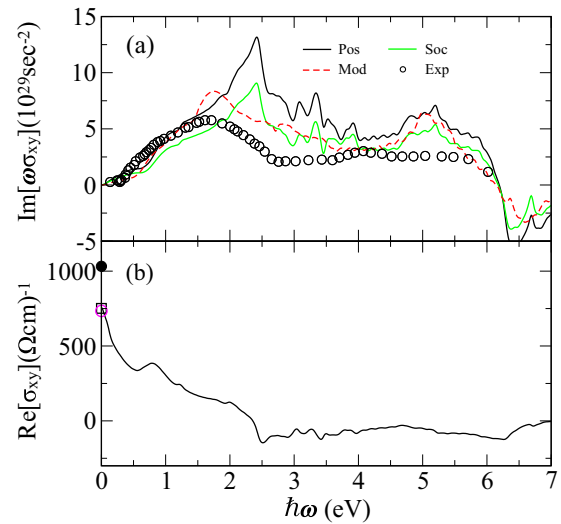


FIG. 2. Frequency-dependent Hall conductivity in bcc Fe. (a) The imaginary part of $\omega\sigma_{xy}$, the magnetic circular dichroism spectrum, is compared with the experimental data presented by open circles from Ref. [28] (Exp) as reproduced in Ref. [15] and Ref. [16]. The black curve shows the result calculated using Eqs. (1) and (7) (Pos), and the green curve shows the result by allowing only 70% strength of the spin-orbit coupling in the d orbitals (Soc). The result obtained from the modified band structure with rescaled hopping integrals between d orbitals (80%) and adjusted onsite energies is presented by the red dashed line (Mod). (b) The real part of σ_{xy} is shown and compared with the dc experiment value [27] (solid circle) and the theoretical results for 0 K (open square) and 300 K (open circle), as discussed in Ref. [15].

with the available theoretical and experimental results. As shown in Fig. 2(a), the curve delivered by Eq. (7) is consistent with other first-principles calculations [15,16], where the spectrum is in good agreement with experiment [28] up to about 1.7 eV. The details of the first-principles results at higher frequencies [15,16], such as the prominent peak at ~ 2.4 eV and a big drop around 6.5 eV, are also well reproduced in our calculations. The real part of the Hall conductivity, as shown in Fig. 2(b), also agrees very well with the reported one [15], such as the dc limit result and the dip at ~ 2.5 eV. Overall, our calculated real and imaginary parts of Hall conductivity, which should satisfy a Kramers-Kronig relation, using Eq. (7) are in good agreement with the reported theoretical and experimental data [15,16,27–30]. We attribute the small errors to the hard Fe pseudopotential that is close to the full potential in our calculations.

Although the general behavior of the conductivity can be described by GGA, the calculated intensity shown in Fig. 2(a) is overall higher than the experimental data at energy > 1.7 eV, which is consistent with the previous findings [15,16]. Since the intensity is related to the strength of spin-orbit coupling, we have calculated the magnetic circular dichroism spectrum by allowing only 70% strength of the spin-orbit coupling for the d orbitals in the self-consistent calculation. As expected, the suppressed spin-orbit coupling lowers the intensity towards the experimental data as shown by the green curve in Fig. 2(a). However, the calculated prominent peak still remains at ~ 2.4 eV, which deviates from the experimental data having the highest intensity at ~ 1.7 eV, and it seems unlikely to reach the 30% error in the spin-orbit coupling. This suggests that a more complete description of many-body Coulomb interactions is needed even in the metallic bcc Fe. The peak at 2.4 eV can be understood from the large number of unoccupied e_g states around 2 eV as shown in Fig. 1 that provides a channel for electrons to excite to. The energy of the flatter occupied e_g states corresponding to larger density of states can be found to be lower than -0.4 eV, and therefore the occupied t_{2g} states have also largely contributed to the peak at 2.4 eV. To simultaneously lower the overall intensity and shift the highest intensity in the calculated spectrum, the Coulomb correlations beyond GGA among all of the Fe $3d$ orbitals should be taken into account.

To compare with the measured bands of bcc Fe in the angle-resolved photoelectron spectroscopy experiments, significant bandwidth renormalization needs to be introduced to the first-principles band structures [17,18]. The bandwidth renormalization is a signature of strong Coulomb correlations and can be described by the Gutzwiller density functional theory, which has revealed a large bandwidth reduction in bcc Fe, for example, by 36% at the H point [17,18]. We therefore have rescaled the hopping integrals between the d orbitals by 80% and adjusted the onsite energies of e_g and t_{2g} orbitals to reach consistent Γ -point band energies calculated by the Gutzwiller density functional theory [18]. The modified band structure is presented by the black curves in Fig. 1. We note that this simple modification of our tight-binding Hamiltonian cannot reproduce the same Fermi surface as the ones calculated by GGA and the Gutzwiller density functional theory, and the modification gives a slightly electron-doped system ($\sim 0.07e$) using the GGA chemical potential. But the modified

tight-binding Hamiltonian can reflect the effect of bandwidth renormalization in the calculated spectrum of magnetic circular dichroism. The result is presented by the red dashed curve in Fig. 2(a), where the lowered overall intensity and the shifted highest intensity towards the experimental data can be identified. This suggests that the magnetic circular dichroism experiment has also evidenced the effect of strong Coulomb correlations in bcc Fe. We expect that an even better improvement can be achieved by considering the many-body Coulomb interactions in the electron-hole channel, which is beyond the scope of this study and should be left for a future work.

IV. SUMMARY

The tight-binding representation of momentum matrix elements for calculating the optical conductivity based on the Kubo-Greenwood formula using the bases of atomic orbitals, where the orthonormal relation is not assumed, is derived. To reach the exact value of the momentum matrix element in the tight-binding representation, the k -dependent position matrix element via Fourier transform needs to be taken into account, which is also needed in an orthonormal basis as well. For the tight-binding parameters obtained from a fitting procedure, the position matrix elements are unknown due to lacking the knowledge of the basis functions and must be parameterized. For the case where the tight-binding Hamiltonian is obtained from first-principles calculations using atomic basis functions, the position matrix elements can be easily calculated since the atomic basis functions are generated at the step of generating the pseudopotentials. Once the geometrical structure is determined, the computational effort for calculating the position matrix elements is similar to the calculation of overlap matrix elements.

Although the number of pseudoatomic orbitals in first-principles calculations is commonly larger than that of the energy-resolved Wannier functions, they share the same advantage of calculating the eigenstates at a dense grid of k points by diagonalizing a tight-binding Hamiltonian in comparison with the plane-wave calculations. Upon finishing self-consistent first-principles calculations using atomic basis functions, such as those implemented in SIESTA [35], Conquest [36], FHI-AIMS [37], CP2K [38], and Atomistix ToolKit [39], a tight-binding Hamiltonian is straightforwardly obtained as well as the other needed ingredients for Eq. (7) and therefore can benefit from our formula. We have studied the frequency-dependent Hall conductivity in ferromagnetic bcc Fe and demonstrated that the results are in good agreement with the reported theoretical and experimental data. By introducing a reasonable bandwidth renormalization by simply rescaling the hopping integrals, better agreement with experiments can be reached, evidencing the effect of strong correlation among $3d$ orbitals in bcc Fe. We therefore propose that the derived formula, which is applicable to a nonorthogonal basis, is useful for studying the optical conductivity using the tight-binding representation.

ACKNOWLEDGMENTS

This work was supported by Priority Issue (creation of new functional devices and high-performance materials to support

next-generation industries) to be tackled by using Post ‘K’ Computer, Ministry of Education, Culture, Sports, Science and Technology, Japan.

APPENDIX: DERIVATION OF MOMENTUM MATRIX ELEMENT IN NONORTHOGONAL BASIS

The energy eigenstate $|\vec{k}n\rangle$ can be expanded by the coefficient of linear combination of atomic orbital, $C_N^{\vec{k}n}$, and $|\vec{k}N\rangle$ can be expressed by $|\vec{R}N\rangle$ via Fourier transform:

$$\begin{aligned} |\vec{k}n\rangle &= \sum_N C_N^{\vec{k}n} |\vec{k}N\rangle \\ &= \sum_{\vec{R}N} \frac{e^{i\vec{k}\cdot\vec{R}}}{\sqrt{N_k}} C_N^{\vec{k}n} |\vec{R}N\rangle. \end{aligned} \quad (\text{A1})$$

The momentum matrix element $\langle \vec{k}m | \hat{p} | \vec{k}n \rangle$ becomes:

$$\begin{aligned} \langle \vec{k}m | \hat{p} | \vec{k}n \rangle &= i \langle \vec{k}m | (\hat{H}\hat{r} - \hat{r}\hat{H}) | \vec{k}n \rangle \\ &= \frac{i}{N_k} \sum_{\vec{R}N\vec{R}'M} C_M^{\vec{k}m*} C_N^{\vec{k}n} e^{i\vec{k}\cdot(\vec{R}-\vec{R}')} \\ &\quad \times \langle \vec{R}'M | (\hat{H}\hat{r} - \hat{r}\hat{H}) | \vec{R}N \rangle, \end{aligned} \quad (\text{A2})$$

where $m_e = 1$ and $\hbar = 1$ have been adopted for the commutation relation $\hat{p} = im_e/\hbar[\hat{H}, \hat{r}]$. By inserting the identity operator,

$$\hat{1} = \sum_{\vec{R}''M'\vec{R}'''N'} |\vec{R}''M'\rangle S_{\vec{R}''M',\vec{R}'''N'}^{-1} \langle \vec{R}'''N' |, \quad (\text{A3})$$

we obtain

$$\begin{aligned} \langle \vec{k}m | \hat{p} | \vec{k}n \rangle &= \frac{i}{N_k} \sum_{\vec{R}N\vec{R}'M\vec{R}''M'\vec{R}'''N'} C_M^{\vec{k}m*} C_N^{\vec{k}n} e^{i\vec{k}\cdot(\vec{R}-\vec{R}')} \\ &\quad \times \langle \vec{R}'M | \hat{H} | \vec{R}''M' \rangle S_{\vec{R}''M',\vec{R}'''N'}^{-1} \langle \vec{R}'''N' | \hat{r} | \vec{R}N \rangle \\ &\quad - \frac{i}{N_k} \sum_{\vec{R}N\vec{R}'M\vec{R}''M'\vec{R}'''N'} C_M^{\vec{k}m*} C_N^{\vec{k}n} e^{i\vec{k}\cdot(\vec{R}-\vec{R}')} \\ &\quad \times \langle \vec{R}'M | \hat{r} | \vec{R}''M' \rangle S_{\vec{R}''M',\vec{R}'''N'}^{-1} \langle \vec{R}'''N' | \hat{H} | \vec{R}N \rangle. \end{aligned} \quad (\text{A4})$$

Considering the translational symmetry, one can get

$$\begin{aligned} \langle \vec{R}'''N' | \hat{r} | \vec{R}N \rangle &= \langle \vec{R}''' - \vec{R}, N' | (\hat{r} + \vec{R}) | 0N \rangle \\ &= \langle \vec{R}''' - \vec{R}, N' | \hat{r} | 0N \rangle \\ &\quad + \vec{R} S_{\vec{R}''M',\vec{R}'''N'} \end{aligned} \quad (\text{A5})$$

and

$$\begin{aligned} \langle \vec{R}'M | \hat{H} | \vec{R}''M' \rangle &= \langle 0M | (\hat{r} + \vec{R}') | \vec{R}'' - \vec{R}', M' \rangle \\ &= \langle 0M | \hat{r} | \vec{R}'' - \vec{R}', M' \rangle \\ &\quad + \vec{R}' S_{\vec{R}'M,\vec{R}''M'}. \end{aligned} \quad (\text{A6})$$

By further noting that

$$\sum_j S_{ij} S_{jk}^{-1} = \sum_j S_{ij}^{-1} S_{jk} = \delta_{ik}, \quad (\text{A7})$$

Eq. (A4) can be rewritten as

$$\begin{aligned} \langle \vec{k}m | \hat{p} | \vec{k}n \rangle &= \frac{i}{N_k} \sum_{\vec{R}N\vec{R}'M} C_M^{\vec{k}m*} C_N^{\vec{k}n} e^{i\vec{k}\cdot(\vec{R}-\vec{R}')} (\vec{R} - \vec{R}') \langle \vec{R}'M | \hat{H} | \vec{R}N \rangle \\ &\quad + \frac{i}{N_k} \sum_{\vec{R}N\vec{R}'M\vec{R}''M'\vec{R}'''N'} C_M^{\vec{k}m*} C_N^{\vec{k}n} e^{i\vec{k}\cdot(\vec{R}-\vec{R}')} \\ &\quad \times \langle \vec{R}'M | \hat{H} | \vec{R}''M' \rangle S_{\vec{R}''M',\vec{R}'''N'}^{-1} \langle \vec{R}'''N' - \vec{R}, N' | \hat{r} | 0N \rangle \\ &\quad - \frac{i}{N_k} \sum_{\vec{R}N\vec{R}'M\vec{R}''M'\vec{R}'''N'} C_M^{\vec{k}m*} C_N^{\vec{k}n} e^{i\vec{k}\cdot(\vec{R}-\vec{R}')} \\ &\quad \times \langle 0M | \hat{r} | \vec{R}'' - \vec{R}', M' \rangle S_{\vec{R}''M',\vec{R}'''N'}^{-1} \langle \vec{R}'''N' | \hat{H} | \vec{R}N \rangle. \end{aligned} \quad (\text{A8})$$

The first term of the right-hand side of Eq. (A8) can be recognized as the derivative of the Hamiltonian matrix element with respect to \vec{k} :

$$\begin{aligned} \frac{\partial}{\partial \vec{k}} (\langle \vec{k}M | \hat{H} | \vec{k}N \rangle) &= \sum_{\vec{R}\vec{R}'} \frac{\partial}{\partial \vec{k}} \frac{e^{i\vec{k}\cdot(\vec{R}-\vec{R}')}}{N_k} \langle \vec{R}'M | \hat{H} | \vec{R}N \rangle \\ &= \sum_{\vec{R}\vec{R}'} i(\vec{R} - \vec{R}') \frac{e^{i\vec{k}\cdot(\vec{R}-\vec{R}')}}{N_k} \langle \vec{R}'M | \hat{H} | \vec{R}N \rangle. \end{aligned} \quad (\text{A9})$$

The second and third terms on the right-hand side of Eq. (A8) can be simplified by considering Eq. (A1), Eq. (A7), and

$$\langle \vec{k}m | \hat{H} = \langle \vec{k}m | \epsilon_{\vec{k}m} \quad (\text{A10})$$

or

$$\hat{H} | \vec{k}n \rangle = \epsilon_{\vec{k}n} | \vec{k}n \rangle. \quad (\text{A11})$$

The momentum matrix element can then be reformulated as

$$\begin{aligned} \langle \vec{k}m | \hat{p} | \vec{k}n \rangle &= \sum_{MN} C_M^{\vec{k}m*} C_N^{\vec{k}n} \frac{\partial}{\partial \vec{k}} (\langle \vec{k}M | \hat{H} | \vec{k}N \rangle) \\ &\quad + \frac{i\epsilon_{\vec{k}m}}{N_k} \sum_{\vec{R}N\vec{R}'M} C_M^{\vec{k}m*} C_N^{\vec{k}n} e^{i\vec{k}\cdot(\vec{R}-\vec{R}')} \langle \vec{R}' - \vec{R}, M | \hat{r} | 0N \rangle \\ &\quad - \frac{i\epsilon_{\vec{k}n}}{N_k} \sum_{\vec{R}N\vec{R}'M} C_M^{\vec{k}m*} C_N^{\vec{k}n} e^{i\vec{k}\cdot(\vec{R}-\vec{R}')} \langle 0M | \hat{r} | \vec{R} - \vec{R}', N \rangle. \end{aligned} \quad (\text{A12})$$

After considering translational symmetry, we obtain an expression by assuming that $\langle 0M | \hat{H} | \vec{R}N \rangle$ and $\langle 0M | \hat{r} | \vec{R}N \rangle$ are known:

$$\begin{aligned} \langle \vec{k}m | \hat{p} | \vec{k}n \rangle &= i \sum_{MN} C_M^{\vec{k}m*} C_N^{\vec{k}n} \sum_{\vec{R}} \langle 0M | \hat{H} | \vec{R}N \rangle \vec{R} e^{i\vec{k}\cdot\vec{R}} \\ &\quad + i\epsilon_{\vec{k}m} \sum_{MN} C_M^{\vec{k}m*} C_N^{\vec{k}n} \left(\sum_{\vec{R}} \langle 0N | \hat{r} | \vec{R}M \rangle e^{i\vec{k}\cdot\vec{R}} \right)^* \\ &\quad - i\epsilon_{\vec{k}n} \sum_{MN} C_M^{\vec{k}m*} C_N^{\vec{k}n} \sum_{\vec{R}} \langle 0M | \hat{r} | \vec{R}N \rangle e^{i\vec{k}\cdot\vec{R}}. \end{aligned} \quad (\text{A13})$$

Alternatively, the second term of the right-hand side of Eq. (A13) can be expressed as

$$i\epsilon_{\vec{k}m} \sum_{MN} C_M^{\vec{k}m*} C_N^{\vec{k}n} \sum_{\vec{R}} \langle \vec{R}M | \hat{r} | 0N \rangle e^{-i\vec{k}\cdot\vec{R}} = i\epsilon_{\vec{k}m} \sum_{MN} C_M^{\vec{k}m*} C_N^{\vec{k}n} \sum_{\vec{R}} \langle 0M | (\hat{r} - \vec{R}) | \vec{R}N \rangle e^{i\vec{k}\cdot\vec{R}}, \quad (\text{A14})$$

and then Eq. (A13) can be written as

$$\begin{aligned} \langle \vec{k}m | \hat{p} | \vec{k}n \rangle &= \sum_{MN} C_M^{\vec{k}m*} C_N^{\vec{k}n} \sum_{\vec{R}} \langle 0M | \hat{H} | \vec{R}N \rangle i\vec{R} e^{i\vec{k}\cdot\vec{R}} + i(\epsilon_{\vec{k}m} - \epsilon_{\vec{k}n}) \sum_{MN} C_M^{\vec{k}m*} C_N^{\vec{k}n} \sum_{\vec{R}} \langle 0M | \hat{r} | \vec{R}N \rangle e^{i\vec{k}\cdot\vec{R}} \\ &\quad - \epsilon_{\vec{k}m} \sum_{MN} C_M^{\vec{k}m*} C_N^{\vec{k}n} \sum_{\vec{R}} \langle 0M | \vec{R}N \rangle i\vec{R} e^{i\vec{k}\cdot\vec{R}}. \end{aligned} \quad (\text{A15})$$

The above equation can also be simply expressed as

$$\langle \vec{k}m | \hat{p} | \vec{k}n \rangle = \sum_{MN} C_M^{\vec{k}m*} C_N^{\vec{k}n} \left(\frac{\partial H_{MN}(\vec{k})}{\partial \vec{k}} - \epsilon_{\vec{k}m} \frac{\partial S_{MN}(\vec{k})}{\partial \vec{k}} \right) + i(\epsilon_{\vec{k}m} - \epsilon_{\vec{k}n}) \sum_{MN} C_M^{\vec{k}m*} C_N^{\vec{k}n} \sum_{\vec{R}} \langle 0M | \hat{r} | \vec{R}N \rangle e^{i\vec{k}\cdot\vec{R}}. \quad (\text{A16})$$

For the special case of $m = n$, Eq. (A16) is reduced to

$$\langle \vec{k}n | \hat{p} | \vec{k}n \rangle = \sum_{MN} C_M^{\vec{k}n*} C_N^{\vec{k}n} \left(\frac{\partial H_{MN}(\vec{k})}{\partial \vec{k}} - \epsilon_{\vec{k}n} \frac{\partial S_{MN}(\vec{k})}{\partial \vec{k}} \right), \quad (\text{A17})$$

which is exactly $\partial\epsilon_{\vec{k}n}/\partial\vec{k}$.

Finally, we demonstrate that the second term of the right-hand side of Eq. (A15) does not depend on the choice of the origin as long as the energy eigenstates are orthogonal to each other, namely $\langle \vec{k}m | \vec{k}n \rangle = 0$ for $m \neq n$, and it is clear that the first and third terms are origin independent due to the relative vector \vec{R} . In the calculation of $\langle 0M | \hat{r} | \vec{R}N \rangle$ in two

coordinate systems whose origins differ by a constant vector \vec{d} , a difference can appear:

$$\langle 0M | \hat{r}_2 | \vec{R}N \rangle = \langle 0M | \hat{r}_1 | \vec{R}N \rangle + \vec{d} \langle 0M | \vec{R}N \rangle. \quad (\text{A18})$$

As a result, an apparent difference for calculating $\langle \vec{k}m | \hat{p} | \vec{k}n \rangle$ in Eq. (A15) can be found as

$$i\vec{d}(\epsilon_{\vec{k}m} - \epsilon_{\vec{k}n}) \sum_{MN} C_M^{\vec{k}m*} C_N^{\vec{k}n} \sum_{\vec{R}} \langle 0M | \vec{R}N \rangle e^{i\vec{k}\cdot\vec{R}}. \quad (\text{A19})$$

However, following Eq. (A1), Eq. (A19) is just the representation of $\langle \vec{k}m | \vec{k}n \rangle$ in real space regardless of a constant factor of $i\vec{d}(\epsilon_{\vec{k}m} - \epsilon_{\vec{k}n})$ and must be zero.

-
- [1] P. Hohenberg and W. Kohn, *Phys. Rev.* **136**, B864 (1964).
[2] W. Kohn and L. J. Sham, *Phys. Rev.* **140**, A1133 (1965).
[3] R. Car and M. Parrinello, *Phys. Rev. Lett.* **55**, 2471 (1985).
[4] M. C. Payne, M. P. Teter, D. C. Allan, T. A. Arias, and J. D. Joannopoulos, *Rev. Mod. Phys.* **64**, 1045 (1992).
[5] M. V. Berry, *Proc. R. Soc. Lond. A* **392**, 45 (1984).
[6] D. J. Thouless, M. Kohmoto, M. P. Nightingale, and M. den Nijs, *Phys. Rev. Lett.* **49**, 405 (1982).
[7] X. Wang, J. R. Yates, I. Souza, and D. Vanderbilt, *Phys. Rev. B* **74**, 195118 (2006).
[8] N. Nagaosa, J. Sinova, S. Onoda, A. H. MacDonald, and N. P. Ong, *Rev. Mod. Phys.* **82**, 1539 (2010).
[9] D. Xiao, M.-C. Chang, and Q. Niu, *Rev. Mod. Phys.* **82**, 1959 (2010).
[10] L. C. Lew Yan Voon and L. R. Ram-Mohan, *Phys. Rev. B* **47**, 15500 (1993).
[11] M. Graf and P. Vogl, *Phys. Rev. B* **51**, 4940 (1995).
[12] T. G. Pedersen, K. Pedersen, and T. Brun Kristensen, *Phys. Rev. B* **63**, 201101(R) (2001).
[13] T. Sandu, *Phys. Rev. B* **72**, 125105 (2005).
[14] J. P. Perdew, K. Burke, and M. Ernzerhof, *Phys. Rev. Lett.* **77**, 3865 (1996).
[15] Y. Yao, L. Kleinman, A. H. MacDonald, J. Sinova, T. Jungwirth, D.-s. Wang, E. Wang, and Q. Niu, *Phys. Rev. Lett.* **92**, 037204 (2004).
[16] J. R. Yates, X. Wang, D. Vanderbilt, and I. Souza, *Phys. Rev. B* **75**, 195121 (2007).
[17] J. Schäfer, M. Hoinkis, E. Rotenberg, P. Blaha, and R. Claessen, *Phys. Rev. B* **72**, 155115 (2005).
[18] T. Schickling, J. Bünemann, F. Gebhard, and L. Boeri, *Phys. Rev. B* **93**, 205151 (2016).
[19] R. Kubo, *J. Phys. Soc. Jpn* **12**, 570 (1957).
[20] D. Greenwood, *Proc. Phys. Soc.* **71**, 585 (1958).
[21] J. Sinova, T. Jungwirth, J. Kučera, and A. H. MacDonald, *Phys. Rev. B* **67**, 235203 (2003).
[22] P. B. Allen, *Contemporary Concepts of Condensed Matter Science*, Vol. 2 of Conceptual Foundations of Materials: A Standard Model for Ground- and Excited-State Properties (Elsevier, Amsterdam, 2006), pp. 165–218.
[23] L. Calderin, V. Karasiev, and S. Trickey, *Comput. Phys. Commun.* **221**, 118 (2017).
[24] M. Menon and K. R. Subbaswamy, *Phys. Rev. B* **47**, 12754 (1993).
[25] A. J. Read and R. J. Needs, *Phys. Rev. B* **44**, 13071 (1991).
[26] H. Kageshima and K. Shiraiishi, *Phys. Rev. B* **56**, 14985 (1997).

- [27] P. N. Dheer, *Phys. Rev.* **156**, 637 (1967).
- [28] G. S. Krinchik and V. A. Artem'ev, *Zh. Eksp. Teor. Fiz.* **53**, 1901 (1967) [*Sov. Phys. JETP* **26**, 1080 (1968)].
- [29] G. Y. Guo and H. Ebert, *Phys. Rev. B* **51**, 12633 (1995).
- [30] N. Mainkar, D. A. Browne, and J. Callaway, *Phys. Rev. B* **53**, 3692 (1996).
- [31] The code, OpenMX, pseudoatomic basis functions, and pseudopotentials are available on a website <http://www.openmx-square.org/>.
- [32] G. Theurich and N. A. Hill, *Phys. Rev. B* **64**, 073106 (2001).
- [33] I. Morrison, D. M. Bylander, and L. Kleinman, *Phys. Rev. B* **47**, 6728 (1993).
- [34] T. Ozaki, *Phys. Rev. B* **67**, 155108 (2003).
- [35] J. M. Soler, E. Artacho, J. D. Gale, A. García, J. Junquera, P. Ordejón, and D. Sánchez-Portal, *J. Phys.: Condens. Matter* **14**, 2745 (2002).
- [36] M. Gillan, D. Bowler, A. Torralba, and T. Miyazaki, *Comput. Phys. Commun.* **177**, 14 (2007).
- [37] V. Blum, R. Gehrke, F. Hanke, P. Havu, V. Havu, X. Ren, K. Reuter, and M. Scheffler, *Comput. Phys. Commun.* **180**, 2175 (2009).
- [38] J. Hutter, M. Iannuzzi, F. Schiffmann, and J. VandeVondele, *Wiley Interdisciplinary Reviews: Computational Molecular Science* **4**, 15 (2014).
- [39] The information for Atomistix ToolKit can be found on a website <http://www.quantumwise.com/>.